

Effect of variations in terminal contact resistances on the current distribution in high-temperature superconducting cables

G P Willering^{1,2}, D C van der Laan^{3,4}, H W Weijers¹, P D Noyes¹,
G E Miller¹ and Y Viouchkov¹

¹National High Magnetic Field Laboratory, Florida State University, Tallahassee, FL, USA

²CERN, Geneva, Switzerland

³Advanced Conductor Technologies LLC, Boulder, Colorado, USA

⁴University of Colorado, Boulder, Colorado, USA

E-mail: gerard.willering@cern.ch

Received 22 September 2014, revised 11 November 2014

Accepted for publication 13 November 2014

Published 21 January 2015



Abstract

Future application of high-temperature superconductors in large volume, high field magnets and in magnet current distribution systems requires cabling of RE-Ba₂Cu₃O_{7- δ} coated conductor tapes. The substantial aspect ratio of RE-Ba₂Cu₃O_{7- δ} coated conductors and the highly resistive buffer layers in these tapes make the development of compact and homogeneous cable terminals complex. The contact resistance between individual tapes and the cable terminations of two types of high-temperature superconducting cables was determined at 77 K at relatively low current ramp rates using a non-destructive method. The current distribution between tapes in the cables caused by a variation in contact resistance was calculated with a simple model, which was validated using different experimental methods. The results show that the current distribution at low current ramp rates in cables made from RE-Ba₂Cu₃O_{7- δ} coated conductors is mainly dictated by the variations in contact resistances between tapes in the cable and the cable terminals. Development of practical cable terminals that minimize the variations in contact resistances is therefore instrumental for the successful application of high-temperature superconducting cables in magnets.

Keywords: high-temperature superconductors, superconducting cable, CORC cable, current distribution

1. Introduction

High field magnets made from high-temperature superconductors (HTS) designed to operate at magnetic fields exceeding 20 T are currently being wound from single RE-Ba₂Cu₃O_{7- δ} (REBCO) coated conductor tapes [1] or Bi₂Sr₂CaCu₂O_x (Bi-2212) round wire [2–4]. Winding large magnets from single tapes or wires leads to an increased inductance, high voltages required for fast charging and discharging and very high voltages that develop during a quench. These magnets will also require many internal splices. Magnet cable technology is required for the development of large, practical, low-inductance magnets. Several coated conductor cable approaches are currently under development

for application in high-field magnets. The three main approaches are:

- (1) the Roebel assembled coated conductor (RACC) cable, in which REBCO coated conductors are fully transposed, results in the highest engineering current density J_e for magnetic fields applied parallel to its surface, making them a possible candidate for accelerator-type magnets [5–7].
- (2) The twisted stacked-tape cable (TSTC), in which the tapes are not fully transposed, is suitable for superconducting magnet distribution systems operating in self-field and possibly an acceptable candidate for large-bore magnets [8, 9]. Several variations of the TSTC

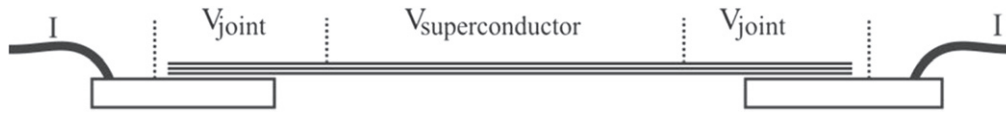


Figure 1. Representation of a cable containing a stack of three tapes soldered to copper terminals, including the voltage contacts covering both terminals and the center superconducting section of the cable. The voltage contacts are represented by the vertical dotted lines in the figure.

cable exist where the stacked tapes are inserted into slotted rods, or sandwiched between copper shells [10, 11].

- (3) The conductor on round core (CORC) cable, in which the tapes are fully transposed within each layer, but not between layers. The high level of flexibility and relatively high J_c at high magnetic fields make CORC cables a suitable candidate for most high-field magnet applications [12–15].

The development of compact cable terminals with equal joint resistances between tapes and terminals is not straightforward and depends on number of tapes in the cable. For the RACC the straightforward soldering of the cable to copper leads results in a symmetric current distribution, when the cable is assembled from a limited number of tapes. In the case of TSTC cables, the straightforward soldering of a stack of coated conductor tapes to a copper lead results in a very asymmetric contact resistance. A more complex termination using a stepwise copper lead or interleaving the tapes with copper or BSCCO tapes may be imperative [8]. In case of CORC cables, soldering the tapes onto the surface of a conical-shaped copper terminal may result in a more even distribution in contact resistance, at least for cables with a limited number of tapes.

The effect of variations in contact resistances on the current distribution in TSTC and CORC cables will be investigated. The current distribution is determined at low current ramp rates using non-destructive methods and by a simple analytical model. The results will provide a first insight of the cable termination performance and how the variation in contact resistance at the terminals influences the current distribution in the cable.

2. Experimental details

2.1. Modeling of current flow in cables

The current distribution between tapes in a superconducting cable can be influenced by:

- quench of one or multiple wires and tapes, resulting in a fast redistribution of current through the current leads or through contacts between tapes.
- Non-uniform joint resistance, resulting in a global (re) distribution of current.
- Non-transposed cables in which variations in magnetic field can lead to local variations in critical current and current distribution.

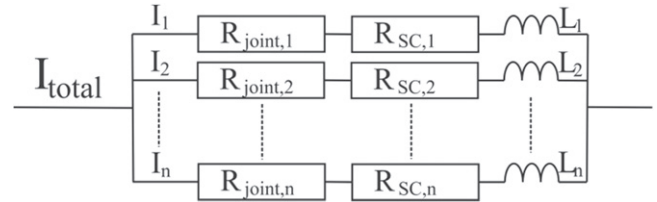


Figure 2. Schematic of parallel current paths used in the model for n tapes.

The focus of this work is on current distribution in HTS cables made from coated conductors, in which current sharing between tapes is neglected because the contact resistance between tapes is relatively high and the cables are relatively short. Current sharing between tapes may play an important role in case the cable is solder-filled, but this is outside the scope of this work. An overview of a cable containing three stacked tapes is shown in figure 1, while the electrical schematic of the parallel current paths of this cable is shown in figure 2.

Equations (1)–(3) present the full description of the voltage over a cable containing n tapes that are soldered to two terminals:

$$V_{\text{total}} = L \frac{dI_i}{dt} + I_i (R_{SC,i} + R_{\text{joint},i}), \quad \text{for } i = 1-n, \quad (1)$$

$$\sum_{i=1}^n I_i = I_{\text{total}}, \quad (2)$$

$$R_{SC,i} = V_c \left(\frac{I_i}{I_{c,i}} \right)^n, \quad \text{for } i = 1-n. \quad (3)$$

Here, I_{total} is the cable current, I_i is the current in tape i , V_{total} is the voltage over the entire cable including the joints with the terminals, $R_{\text{joint},i}$ is the combined joint resistance of tape i to both terminals, $R_{SC,i}$ is the resistance of the superconductor, L_i is the inductance of each current path, V_c is the voltage criterion at which the critical current is defined, and n is the steepness of the superconducting transition. The self and mutual inductances of the tapes are omitted from the equations, because of the slow current ramp rate in the order of 1 A s^{-1} that is applied during these measurements. The equations are solved in an iterative numerical model, during which process the critical current $I_{c,i}$ may vary per tape and depends on the applied magnetic field and the self-field.

2.2. Coated conductor cable samples and terminations

Measurements were performed at three different institutes on three types of coated conductor cables. An overview of the

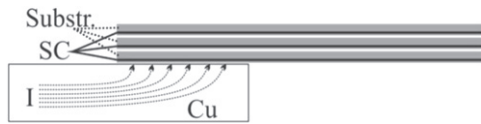


Figure 3. Solder connection of a twisted stacked-tape cable to a simple terminal. The superconducting side of the tapes (SC) is facing the copper terminal.

samples and their terminations is provided in this section. The three samples, including the institutes at which they were measured, are listed in table 1. The cables were prepared from 4 mm wide REBCO coated conductors that contained a $1\ \mu\text{m}$ thick superconducting film that was deposited onto several resistive buffer layers located on a $50\ \mu\text{m}$ thick Hastelloy substrate. The tapes were surround-plated with $20\ \mu\text{m}$ of copper.

2.2.1. Sample 1: TSTC with simple terminals. Sample 1 was formed by stacking three REBCO coated conductors on top of each other and wrapping the stack with Kapton tape. The simplest terminal configuration was chosen, in which the TSTC was soldered directly onto the copper terminals using Sn63Pb37 solder. A high inhomogeneity in joint resistance can be expected, because the superconducting side of the bottom tape was soldered directly onto the copper, while the current from the other two tapes needs to bypass the resistive buffer layers of the tapes, through the copper plating, thereby significantly increasing the contact resistance. Figure 3 shows an overview of the terminal onto which the three tapes were soldered. The joints between tapes and terminal were about 0.1 m in length, while the total cable length was 1 m.

Nine voltage contact pairs were soldered to sample 1, following the overview given by figure 1. Three voltage contact pairs covered the central region of each tape over a length of 0.7 m. Six contact pairs covered the joints between the tapes and the copper terminals, each pair having one voltage tab on the terminal and the other voltage tap on the tape, 15 cm from the joint. This configuration allowed for the measurement of the full voltage across each tape, while allowing for the distinction of the voltages over each joint and the superconductor.

2.2.2. Sample 2: TSTC with interlaced copper terminals. Sample 2 was a non-twisted TSTC cable of 0.61 m in length, containing four tapes and terminals formed by soldering copper tapes interlaced with the superconducting tapes (see figure 4). This cable was prepared and characterized by Dr Takayasu at MIT and in this report the data published in [8] and [9] is further analyzed. This solution gave a symmetric joint with a homogeneous distribution in contact resistances. The characterization also included measuring the current per tape with calibrated Hall sensors and measuring the voltage at the center of each tape.

2.2.3. Sample 3: CORC cable with conical terminals. Sample 3 was a CORC cable consisting of six REBCO coated

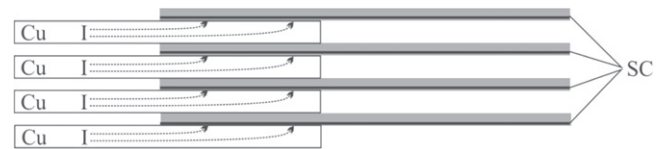


Figure 4. Overview of a cable of sample 2, containing four coated conductor tapes, in which the joint to the terminal was formed by interlacing the superconducting tapes with copper tapes.

conductors that were wound in a helical fashion onto a flexible, round and non-conductive former with a diameter of 5.5 mm. The REBCO coated conductors were wound with their superconducting layer on the inside, facing the former, to take advantage of their ability to sustain relatively large axial compressive strains without mechanical damage [16, 17]. The winding angle of the tapes is between about 36° and 54° as a tradeoff between ease of winding and tape consumption, with the added benefit of having the winding strain oriented as close to the [110] orientation of the superconducting film in the tapes, thereby minimizing the reversible strain effect on I_c [18, 19]. Figure 5 shows a representation of the cable layout. The tapes in sample 3 are soldered to the copper terminations with In–Bi solder. Each tape contained three sets of voltage pairs, as outlined in figure 1. The voltage leads were co-wound with the superconducting tapes in the cable to minimize inductive voltages.

3. Results and discussion

3.1. Determination of the joint resistance in cables

Three methods were used to determine the joint resistance between the tapes and the terminals in a superconducting cable. All methods are indirect because either the current or the voltage per tape is unknown.

- (1) The cables were instrumented with three voltage contact pairs per tape, one pair for each joint and one pair for the superconducting section of the tape. This method required the assumption of the current in the tape at its superconducting transition as will be described below in detail.
- (2) Measuring the self-field of each tape by using a calibrated field measurement setup. The joint resistance per tape can be determined from the current distribution among the tapes and the overall joint resistance [8].
- (3) Cutting the cable after the measurements and measure the joint resistance by powering each tape separately [8]. We did not perform these measurements, but will use data published in [8] in our effort to reanalyze the results.

3.1.1. Method 1: contact resistance determination through voltage measurements. The voltages of samples 1 and 3 were measured at three locations per tape, as outlined in

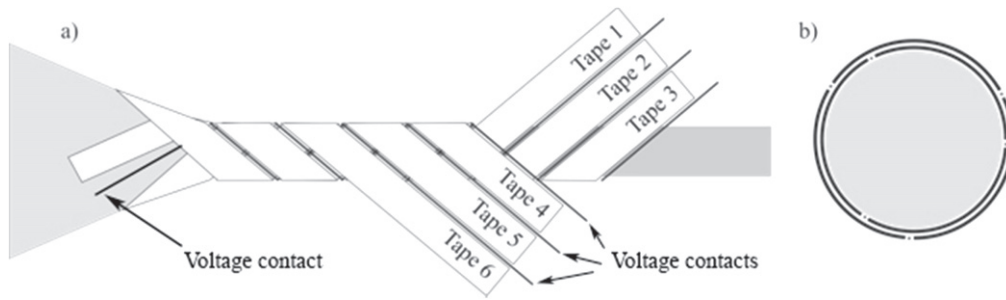


Figure 5. (a) CORC cable with two layers of three tapes each (white) wound around a round former (gray) and connected to conical-shaped copper terminals. Voltage wires (black lines) were wound in the voids between the tapes. (b) Cross-section of the 6-tape cable.

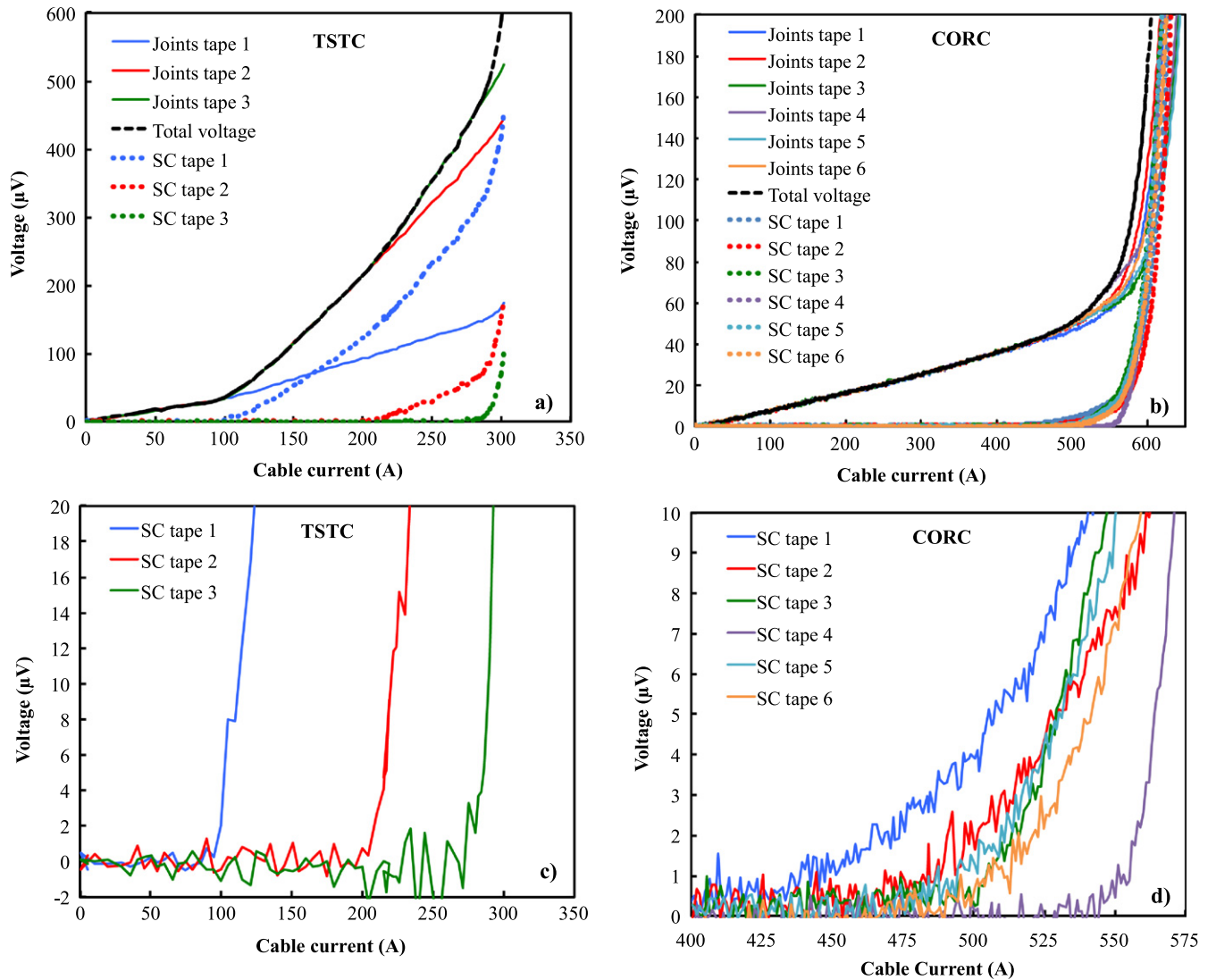


Figure 6. Voltages measured at 77 K during a slow current ramp for (a) sample 1 and (b) sample 3. The black dashed line indicates the total voltage over the cable. Details of voltages measured over the superconducting part of the tapes for (c) sample 1 and (d) sample 3.

Table 1. Overview of the three cables being studied.

Sample	Cable type	Terminal technology	Institute/company
1	Twisted stacked-tape cable	Soldered stack	CERN
2	Twisted stacked-tape cable	Tapes interlaced with Cu tapes	MIT
3	Conductor on round core	Tapes soldered on conical terminal	NHMFL/Advanced Conductor Technologies

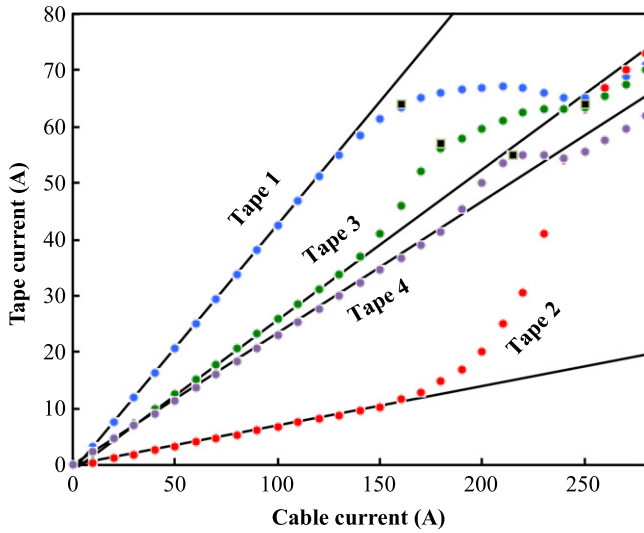


Figure 7. Tape currents for tapes 14 as a function of cable current, determined with Hall probes for sample 2. The solid lines are a curve fit between 0 and 100 A for each tape. The black dots indicate the start of a negative second derivative of the curve. The figure is reprinted from [9].

figure 1 during a slow current ramp rate in liquid nitrogen (see figure 6). The voltages measured over the joints of each tape with the two terminals were added, thereby losing the ability to distinguish between the resistances of both joints, but simplifying the calculation of the current distribution between the tapes. The sum of the three voltages measured on each tape was always equal to V_{total} , illustrated by the measurements in figure 6, where all the joint voltages follow the total voltage (thick dashed line) until the superconductor starts its transition into the normal state. The slope of the total voltage of sample 1 changes significantly at certain cable currents, indicating a change in current distribution between tapes.

The following steps were taken to calculate the total contact resistance between each tape in the cable and its terminals:

- (1) the cable transition current $I_{\text{trans,cable},i}$ was determined for each tape i . $I_{\text{trans,cable},i}$ is defined as the current at the smallest measurable voltage onset of the superconducting section of the tapes. The threshold of $2 \mu\text{V}$ was used for the measurement shown in figure 6.
- (2) The total voltage $V_{\text{total,trans},i}$ was determined at $I_{\text{trans,cable},i}$ for each tape i .
- (3) The current $I_{\text{trans,tape},i}$ in tape i is assumed equal to the maximum $I_{\text{trans,cable},i}$ divided by the number of tapes.
- (4) The contact resistance between each tape and the terminals was calculated from $V_{\text{total,trans},i}$ for each tape i using the tape current $I_{\text{trans,tape},i}$ as calculated during step 3.

The results of steps 1–4 when applied to the measurements outlined in figure 6 are listed in tables 2 and 3 for samples 1 and 3 respectively.

Table 2. Characteristic parameters of sample 1 determined from measurements at 77 K in self field.

Tape	$I_{\text{trans,cable},i}$ (A)	$I_{\text{trans,tape},i}$ (A)	$V_{\text{total,trans},i}$ (μV)	$R_{\text{joint},i}$ ($\text{n}\Omega$)
1	103	95	33	350
2	205	95	215	2270
3	285	95	467	4913

Table 3. Characteristic parameters of sample 3 determined from measurements at 77 K in self field.

Tape	$I_{\text{trans,cable},i}$ (A)	$I_{\text{trans,tape},i}$ (A)	$V_{\text{total,trans},i}$ (μV)	$R_{\text{joint},i}$ ($\text{n}\Omega$)
1	425	93	40	435
2	470	93	47	506
3	495	93	51	554
4	555	93	74	797
5	480	93	49	524
6	505	93	53	577

The contact resistance per tape was very inhomogeneous for sample 1, which can easily be explained by the way how the tapes were soldered onto the terminals. Tape 1 was soldered with its superconducting side directly onto the copper terminal, resulting in a total contact resistance of $350 \text{ n}\Omega$. Tape 2 was soldered on top of tape 1, having the resistive buffer layers of tape 1 partly preventing current from reaching the terminal. Current had to flow around the buffer layers through a thin layer of plated copper, resulting in a much higher contact resistance of $2270 \text{ n}\Omega$. Tape 3 was soldered on top of tape 2 and current had to pass around two tapes with resistive buffer layers, resulting in an even higher contact resistance of $4913 \text{ n}\Omega$.

The variations in contact resistance between the tapes and the terminals were much smaller for sample 3, because all tapes were soldered with their superconductor side directly onto the copper terminals. The relatively small variations in contact resistance ranging from $435 \text{ n}\Omega$ to $797 \text{ n}\Omega$ could be caused by variation in solder area and solder thickness.

The data in figure 6 clearly show that the superconducting to normal transition of the cable when measured by voltage contact on a single tape strongly depends on the tape over which the voltage is measured. The cable critical current can only be determined accurately by measuring the voltages over all tapes, or over the entire cable including its terminals, unless the current distribution is perfectly homogeneous.

3.1.2. Method 2: determination of contact resistance by measuring local magnetic fields. Dr Takayasu showed in [9] that Hall probe measurements of the self-field generated by each tape revealed the current distribution in the 4-tape cable formed by sample 2. Figure 7 shows the current in each tape of sample 2, calculated from the Hall probe measurements published in [9], as a function of cable

Table 4. Ratio of tape currents and joint resistances per tape for sample 2.

Tape	I_i/I_{cable}	$R_{\text{joint},i}/R_{\text{joint,total}}$
1	0.435	2.3
2	0.070	14.3
3	0.265	3.8
4	0.230	4.3

current. The data was re-analyzed as part of this current paper, and the ratio between $R_{\text{joint},i}$ for each tape was calculated directly from the ratio between $I_{\text{tape},i}$ at currents far below I_c , as determined with the Hall probe. Thus:

$$I_1 R_{\text{joint},1} = I_2 R_{\text{joint},2} = I_3 R_{\text{joint},3} = I_4 R_{\text{joint},4}. \quad (4)$$

The ratio of the slopes of each tape between cable current of 0 and 100 A in figure 7 equals the ratio of current in each tape. The current ratios and the accompanying resistance ratios for each tape in sample 2 are listed in table 4. The total joint resistance is not measured for this sample, but it will be deduced from the measured voltages in the superconducting tape in section 3.2.2.

Additional information about the current distribution in sample 2 can be obtained from the second derivative of the tape current shown in figure 7, since it will become negative when the superconductor starts to transition. This change is indicated in figure 7 by black dots at a tape current of 64, 64, 57 and 55 A for tape 1–4, respectively. The change of derivative provides us with information about the ratio between the critical currents of each tape. In case of sample 2, the sum of the values was 240 A, which was 13 A lower than the cable I_c . The I_c s of each tape were estimated at 68, 68, 60.6, 58.4 A for tapes 1, 2, 3 and 4, respectively. The current in tape 4 was significantly lower than the current in the other tapes at cable currents above 250 A, showing that the tape has, at least locally, a lower I_c .

3.1.3. Method 3: *ex situ* direct resistance measurement. The current through each tape can be obtained and the contact resistance can be measured directly by powering each tape individually. This method typically requires cutting the tapes as was done for sample 2 [5] (see table 5). A large discrepancy was found between the contact resistance ratios as determined with method 2, compared to method 3. One can conclude that the given resistance has at least a certain offset, because the joint resistance measurements include a part of the copper leads that act as a common resistance for all tapes.

3.2. Modeling the current distribution in HTS cables

3.2.1. Sample 1: TSTC with simple terminals. The characteristic parameters obtained for sample 1 and listed in table 2 provide the input for the model to calculate the current distribution in the cable, as outlined by equations (1)–(3). The voltage versus current characteristics measured on the three tapes of sample 1 are compared with the model in figure 8(a). The model is in good agreement with the measurement, since

Table 5. Joint resistance for each tape in sample 2, measured after the tapes have been cut, data from [5].

Tape	$R_{\text{joint},i} (\mu\Omega)$	$R_{\text{joint},i}/R_{\text{joint,total}}$
1	0.67	3.6
2	1.06	5.7
3	0.65	3.5
4	0.73	3.9

the only fitting parameter used was the fraction of resistance per tape as a function of the total resistance. The current per tape was calculated and is shown in figure 8(b) as a function of cable current. The large difference in fraction of current per tape is clearly seen, which is caused by the large variation in joint resistances between tapes and terminals. In the first 100 A of cable current the current in tape 1 is 14 times higher than that in tape 3.

3.2.2. Sample 2: TSTC with interlaced copper terminals. The measurement that was performed on sample 2 by Dr Takayasu and published in [9] was not specifically designed to provide the input for our model to calculate the current distribution. In addition, two methods to determine the contact resistance ratios gave different results, while at the same time the overall contact resistance was not measured.

Here we attempt to calculate the current distribution of sample 2 using the input listed in table 4. The results are shown in figure 9(a). The overall joint resistance of 24 n Ω was deduced by fitting the calculated voltages on the superconductors to the measured voltages for cable currents between 200 and 250 A, as outlined in figure 9(b). The resistance per tape was calculated using the ratios listed in table 4, which are 55 n Ω , 343 n Ω , 91 n Ω and 103 n Ω for tape 1, 2, 3 and 4, respectively. One outcome of the model was that, after all tapes had transitioned into the normal state, the current distribution was only defined by the superconducting properties and not the joint resistances. The measured current in tape 4 was reduced the most due to its lower critical current, which was likely due to an overall degradation of the tape or to a self-field effect. The voltages in cable 2 deviated by more than 10 μ V within a given cable current range because of the limited available input for the model.

3.2.3. Sample 3: CORC cable with conical terminals. The voltage contacts in sample 3 were placed as outlined in figure 1 and the overall resistance was measured at 77 K. The resistance ratio was deduced using method 1, resulting in the parameters listed in table 2. A very good agreement between the calculated and measured voltages was obtained (see figure 10(b)). Tapes 1 and 4 had the lowest and highest joint resistances of 0.77 and 1.40 times the average resistance, respectively, which is reflected in the current distribution shown in figure 10(a). A factor of 1.8 between the lowest current flowing in tape 4 and the highest current flowing in tape 1 is a direct result of the difference in contact resistance.

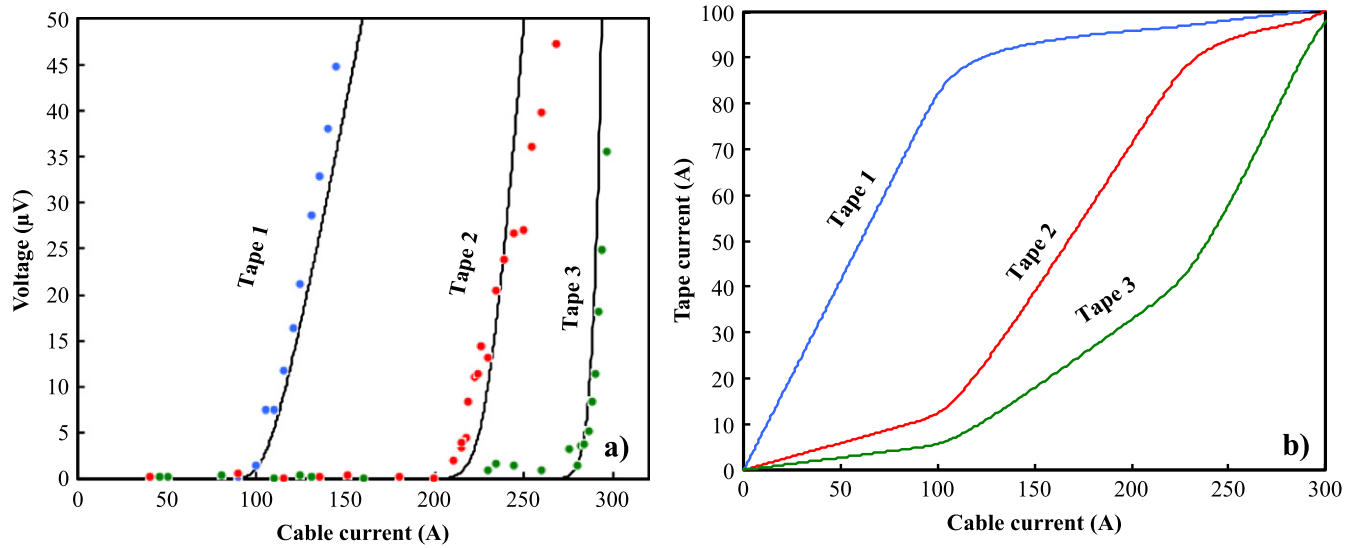


Figure 8. (a) Voltages measured on the three tapes of sample 1 (dots) compared with calculations (lines). (b) The calculated tape current as a function of cable current.

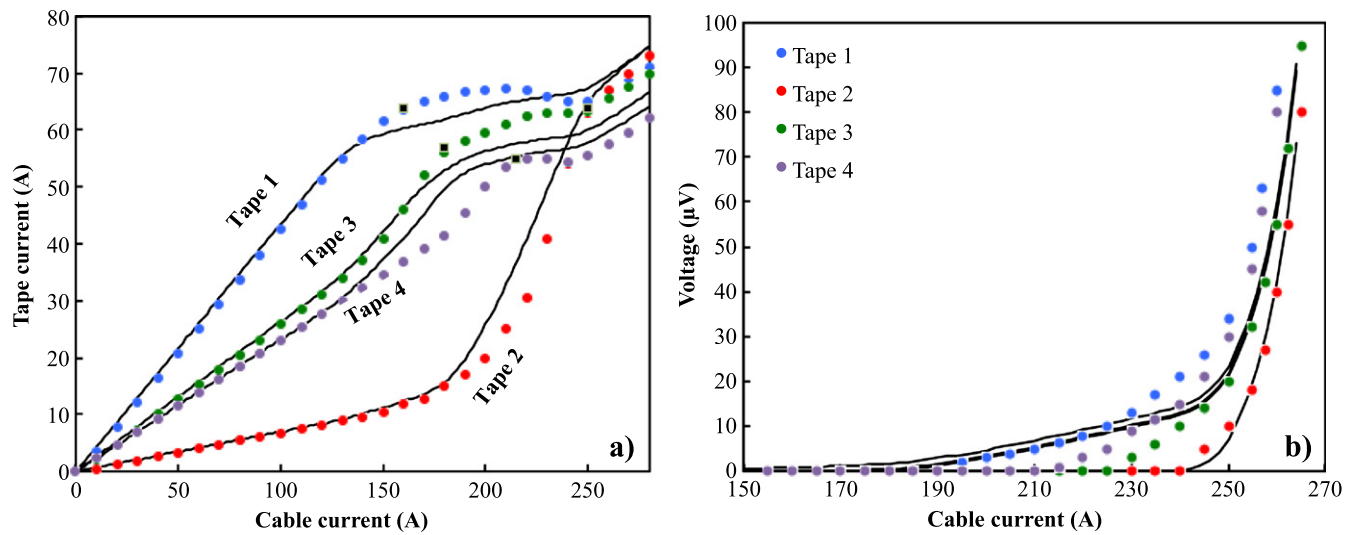


Figure 9. (a) Current measurement and (b) voltage measurements performed on the four tapes of sample 2 (dots), compared with calculations (solid lines). Measurement data reproduced from [9].

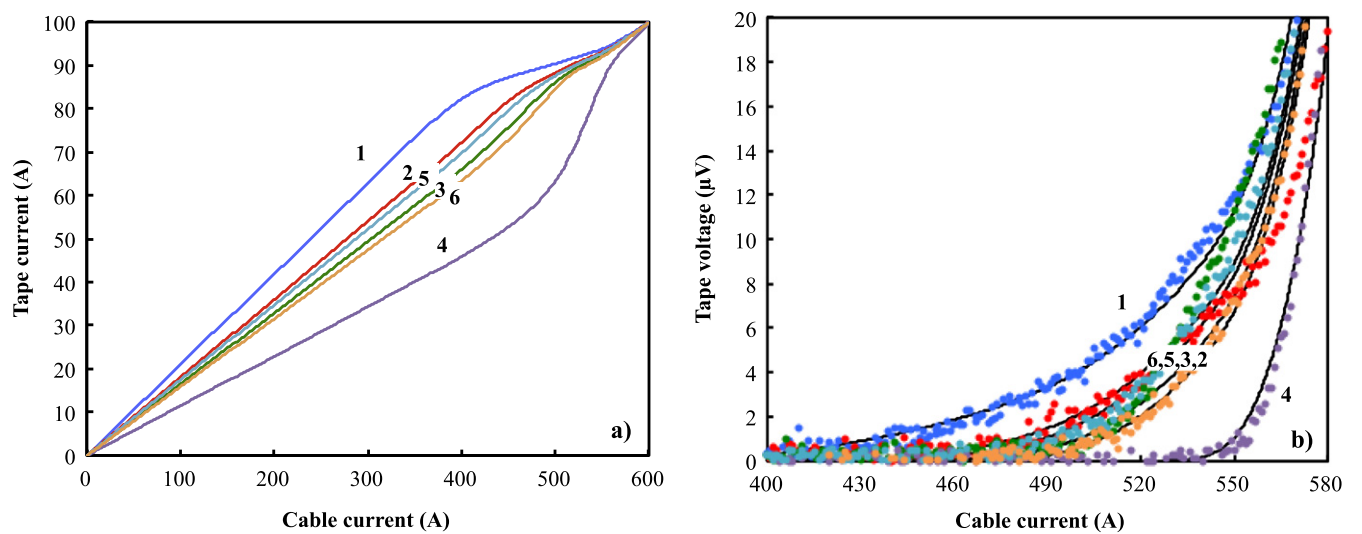


Figure 10. (a) Calculated current and (b) measured (dots) and calculated (lines) voltages of all six tapes of sample 3.

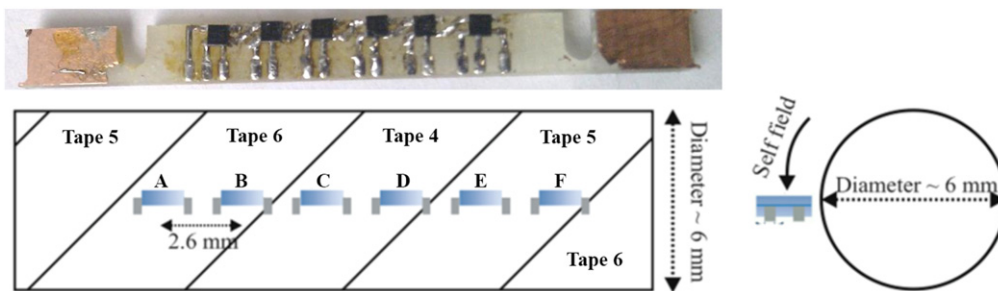


Figure 11. Hall probe array containing six probes and their location next to the tapes of sample 3.

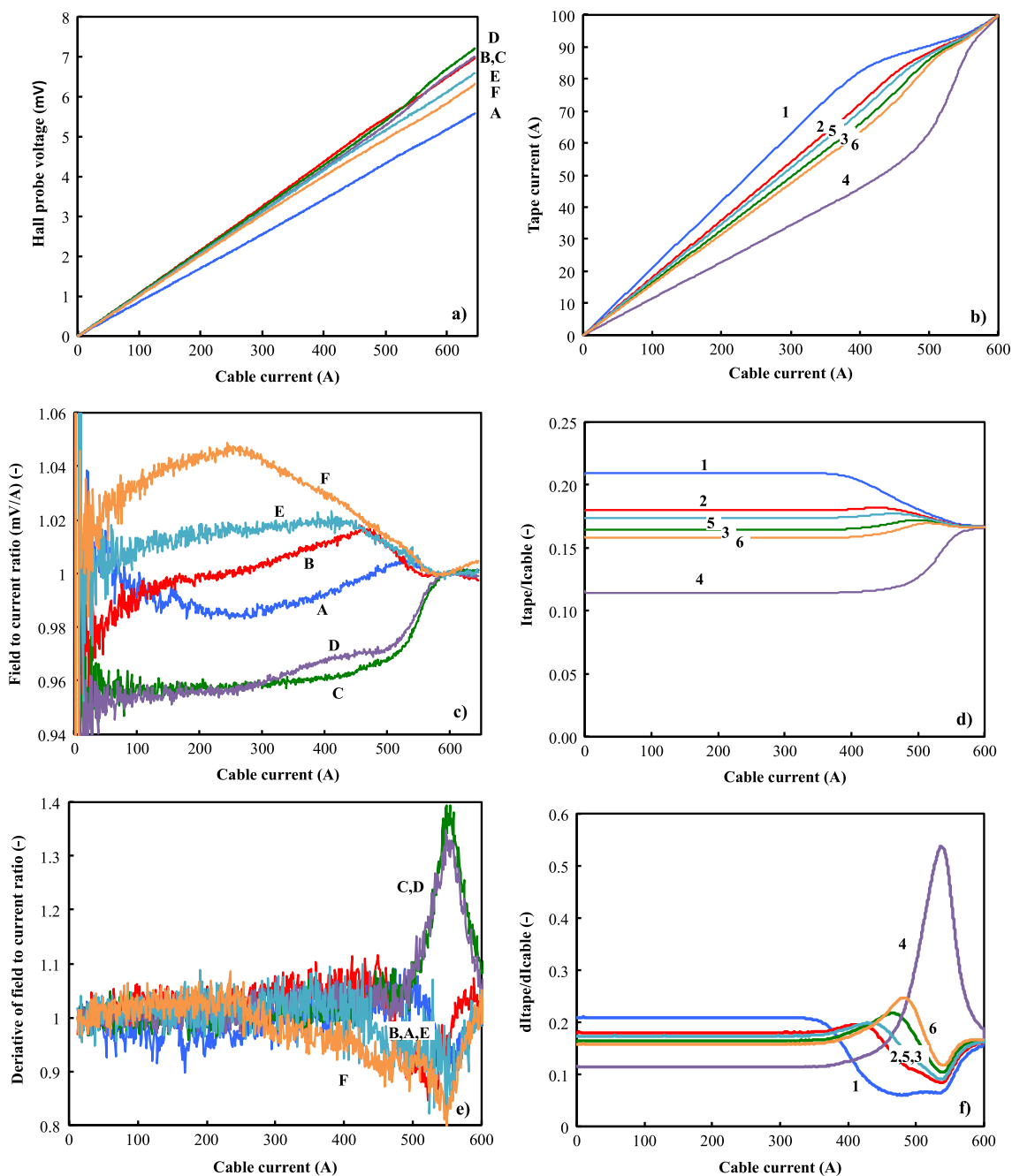


Figure 12. (a) Voltage measured at 77 K using six Hall probes placed near the surface of sample 3. (b) Tape current as a function of cable current as calculated using equations (1)–(3). (c) Field-to-current ratio determined from the Hall probe measurement. (d) Fraction of cable current per tape. (e) Normalized Hall probe field-to-current ratio. (f) First derivative of the current fraction per tape as a function of cable current.

3.3. Detection of current redistribution in CORC cables by use of Hall probes

An array of six Hall probes was placed along the length of the CORC cable (sample 3), such that the azimuthal component of the self-field around the CORC cable could be measured (see figure 11). This non-destructive measurement technique allowed us to obtain the relative variations in current distribution per tape as a function of cable current. The distance between the Hall probes was chosen such that the array of six Hall probes covered one twist pitch of the tapes in the CORC cable. The analysis was conducted on normalized signals since the Hall probes were not calibrated.

The relative current distribution in the three outer tapes of sample 3, as calculated from the Hall probe signals, was compared to the current distribution as calculated in section 3.2.3. The contribution to the magnetic field of the tapes in the inner layer are not taken into account in this comparison. The Hall probe voltages measured as a function of cable current did not show much variation with cable current (see figure 12(a)). The field-to-current ratio of the cable was established by dividing the Hall probe voltages by the cable current. The ratio corresponds to the local current in the cable, and thus the current distribution. It could be normalized by assuming that the current in the cable was evenly distributed when it reached 600 A and when the cable transitioned into its normal state (see figure 12(b)). The change in slope of the field-to-current ratio was emphasized by taking its first derivative (see figure 12(c)). The most striking result was the sudden increase in voltage of Hall probes C and D, positioned directly above tape 4, at a cable current of about 530 A, while the voltage of the other four Hall probes decreased. The increase in Hall probe voltage was the result of a sudden increase in current in tape 4.

The tape current as a function of cable current of sample 3, as shown in figure 10(a), was reproduced in figure 12(d) to allow for a direct comparison between current distribution as determined with the Hall probes and the model. Figure 12(e) shows the fraction $I_{\text{tape}}/I_{\text{cable}}$, showing that tape 1 carries 21% of the cable current, while tape 4 only carries 11% of the current. The voltage buildup due to the superconducting-to-normal transition of the tapes enforces a homogeneous distribution for cable currents exceeding about 500 A. The current in tape 4, having the highest joint resistance to the terminals, increases more rapidly than the current in the other tapes. The second derivative of the Hall probe signals of probe C and D reaches its maximum at a cable current of 540 A. This is the same current at which the calculated second derivative of the current in tape 4 peaks with the input from measurements with method 1. The magnitude at which current in tape 4 increased was much larger than the change in magnitude of the magnetic field near the surface of tape 4, because the local self-field measured near the surface of the cable was also influenced by the current running in the other five tapes of the cable. The measurements of the local self-field of the cable as a function of cable current provided us with a strong validation of the current distribution model that is based on tape voltage measurements.

4. Conclusions

The current distribution in several types of high-temperature superconducting cables containing REBCO coated conductors was determined at low current ramp rates using voltage and Hall probe measurements. The voltages measured over the joints between the tapes in the cable and the cable terminals, together with the voltages measured over each superconducting tape in the cable, were used as input for the model to calculate the current distribution.

The results showed that the current distribution at low current ramp rates, at which the inductance of the tapes does not influence the current distribution, is mainly determined by the difference in contact resistance between the tapes and the cable terminals. The current distribution is relatively inhomogeneous in the presence of large variations in contact resistance, when the higher contact resistance prevents current from entering the tape. The current distribution becomes homogeneous only when the superconducting tapes transition into their normal state. The redistribution of current in the cable causes large changes in slope of the overall cable voltage as a function of current. The change in slope could be used as a first indication that the current distribution in the cable is inhomogeneous.

The current distribution calculated from the voltages measured over the tapes of a CORC cable have been verified by measuring the local self-field of the cable using a Hall probe array, providing a strong validation of the model.

It is concluded that one of the critical design parameters for high field HTS magnet cables is the development of terminals with a uniform joint resistance. Variation in joint resistance will cause a non-uniform current distribution that directly influences the critical current and voltage characteristic of the cable. The cable terminal will thus have a large influence on the field quality of for instance accelerator magnets.

Acknowledgments

The authors kindly acknowledge Dr Takayasu for discussing the results and allowing the use of data from his publications. This work is supported in part by the US Department of Energy, under contract numbers DE-AI05-98OR22652, DE-SC0007891, and DE-SC0007660, the US National Science Foundation under Cooperative Agreement number DMR-0654118 and the State of Florida.

References

- [1] Markiewicz D *et al* 2012 *IEEE Trans. Appl. Supercond.* **22** 4300704
- [2] Weijers H, Trociewitz U, Markiewicz D, Myers D, Hellstrom E, Xu A, Jaroszynski J, Noyes P, Viouchkov Y and Larbalestier D 2010 *IEEE Trans. Appl. Supercond.* **20** 576–82
- [3] Larbalestier D C *et al* 2014 *Nat. Mater.* **13** 375–81

- [4] Trociewitz U P, Dalban-Canassy M, Hannion M, Hilton D K, Jaroszynski J, Noyes P, Viouchkov Y, Weijers H W and Larbalestier D C 2011 *Appl. Phys. Lett.* **99** 202506
- [5] Goldacker W, Nast R, Kotzyba G, Schlachter S, Frank A, Ringsdorf B, Schmidt C and Komarek P 2006 *J. Phys. Conf. Ser.* **43** 901
- [6] Goldacker W, Frank A, Heller R, Ringsdorf B, Weiss K, Schmidt C and Schuller S 2007 *IEEE Trans. Appl. Supercond.* **17** 3396–401
- [7] Goldacker W, Frank A, Kudymow A, Heller R, Kling A, Terzieva S and Schmidt C 2007 *Supercond. Sci. Technol.* **22** 034003
- [8] Takayasu M, Chiesa L, Bromberg L and Minervini J 2012 *Supercond. Sci. Technol.* **25** 014011
- [9] Takayasu M, Chiesa L, Bromberg L and Minervini J 2011 *IEEE Trans. Appl. Supercond.* **21** 2340–4
- [10] Uglietti D, Wesche R and Bruzzone P 2014 *IEEE Trans. Appl. Supercond.* **24** 4800704
- [11] Celentano G, De Marzi G, Fabbri F, Muzzi L, Tomassetti G, Anemona A, Chiarelli S, Seri M, Bragagni A and della Corte A 2014 *IEEE Trans. Appl. Supercond.* **24** 4601805
- [12] van der Laan D C 2009 *Supercond. Sci. Technol.* **22** 065013
- [13] van der Laan D C, Goodrich L and Haugan T 2012 *Supercond. Sci. Technol.* **25** 014003
- [14] van der Laan D C, Lu X and Goodrich L 2011 *Supercond. Sci. Technol.* **24** 042001
- [15] van der Laan D C, Noyes P, Miller G, Weijers H and Willering G 2013 *Supercond. Sci. Technol.* **26** 045005
- [16] van der Laan D C and Ekin J W 2007 *Appl. Phys. Lett.* **90** 052506
- [17] van der Laan D C, Ekin J W, Douglas J F, Clickner C C, Stauffer T C and Goodrich L F 2010 *Supercond. Sci. Technol.* **23** 072001
- [18] van der Laan D C, Abraimov D, Polyanskii A A, Larbalestier D C, Douglas J F, Semerad R and Bauer M 2011 *Supercond. Sci. Technol.* **24** 115010
- [19] van der Laan D C, Douglas J F, Goodrich L F, Semerad R and Bauer M 2012 *IEEE Trans. Appl. Supercond.* **22** 8400707